View metadata, citation and similar papers at core.ac.uk

brought to you by CORE

provided by Research Online

University of Wollongong

Research Online

Faculty of Engineering and Information Sciences - Papers: Part B

Faculty of Engineering and Information Sciences

2019

Thermionic enhanced heat transfer in electronic devices based on 3D Dirac materials

Sunchao Huang
University of Wollongong, sh676@uowmail.edu.au

R A. Lewis
University of Wollongong, roger@uow.edu.au

C Zhang
University of Wollongong, czhang@uow.edu.au

Follow this and additional works at: https://ro.uow.edu.au/eispapers1

Part of the Engineering Commons, and the Science and Technology Studies Commons

Recommended Citation

Huang, Sunchao; Lewis, R A.; and Zhang, C, "Thermionic enhanced heat transfer in electronic devices based on 3D Dirac materials" (2019). *Faculty of Engineering and Information Sciences - Papers: Part B*. 3349.
https://ro.uow.edu.au/eispapers1/3349

Research Online is the open access institutional repository for the University of Wollongong. For further information contact the UOW Library: research-pubs@uow.edu.au

Thermionic enhanced heat transfer in electronic devices based on 3D Dirac materials

Abstract

We calculate the heat transfer from electronic devices based on three-dimensional Dirac materials without and with thermionic cooling. Without thermionic cooling, the internal temperature of the devices is at best equal to and usually higher than the temperature of the surrounding environment. However, when thermionic cooling is employed to transport heat, the internal temperature can be considerably lower than the environmental temperature. In the proposed thermionic cooling process, the energy efficiency can be as high as 75% of the Carnot efficiency.

Disciplines

Engineering | Science and Technology Studies

Publication Details

Huang, S., Lewis, R. A. & Zhang, C. (2019). Thermionic enhanced heat transfer in electronic devices based on 3D Dirac materials. Japanese Journal of Applied Physics, 126 (16), 165105-1-165105-5.

This journal article is available at Research Online: https://ro.uow.edu.au/eispapers1/3349

Thermionic enhanced heat transfer in electronic devices based on 3D Dirac materials

Sunchao Huang, R. A. Lewis and Chao Zhang[a)]

School of Physics, University of Wollongong, Wollongong, New South Wales 2522, Australia

We calculate the heat transfer from electronic devices based on three-dimensional (3D) Dirac materials without and with thermionic cooling. Without thermionic cooling, the internal temperature of the devices is at best equal to and usually higher than the temperature of the surrounding environment. However, when thermionic cooling is employed to transport heat, the internal temperature can be considerably lower than the environmental temperature. In the proposed thermionic cooling process, the energy efficiency can be as high as 75% of the Carnot efficiency.

[a)] czhang@uow.edu.au

I. INTRODUCTION

The heat power density of electronic devices increases rapidly with their miniaturization and integration, which are the main developments of future devices. The high density of heat power demands more powerful methods to transport heat. Otherwise, a high internal temperature will result. For electronic devices, a high internal temperature reduces not only their efficiency but also their lifetime[1]. There are several cooling schemes to overcome these problems, such as high-flux heat pipes, air-cooled heat sinks, direct liquid immersion and thermionic cooling[2,3]. Thermionic cooling is based on thermionic emission that was discovered by Richardson in 1901. Thermionic emission refers to the process where electrons are driven by thermal energy across a surface barrier, which is a hot research topic[4–8]. For conventional materials with a parabolic energy-momentum dispersion, the thermionic emission density is described by the Richardson-Dushman (RD) law:

$$J_R(T) = \frac{qmk_{\mathrm{B}}^2}{2\pi^2\hbar^3}T^2\mathrm{e}^{-q\phi\beta}, \tag{1}$$

where q is the electron charge, m is the electron mass, k_{B} is the Boltzmann constant, $\hbar$ is the reduced Plank's constant, ϕ is the surface potential and $\beta = 1/(k_{\mathrm{B}}T)$, where T is the thermodynamic temperature. A 3D Dirac semimetal phase with a linear energy-momentum dispersion has been experimentally observed in Cd_3As_2 by means of angle-resolved photoemission spectroscopy[9]. The material has attracted considerable attention[10–13] and has been found to have many astounding properties such as the extraordinarily high mobility of electrons (10,000 cm^2/V s at room temperature)[14], tunable mid-infrared optical switching[15], low thermal conductivity[16] and high efficiency and non-Richardson thermionics[17,18]. By using the linear energy-momentum dispersion, the thermionic emission of Dirac materials is determined to be[17]

$$J(T) = \frac{qk_{\mathrm{B}}^2}{4\pi^2\hbar^3v_{\mathrm{F}}^2}(q\phi + E_{\mathrm{F}} + 2k_{\mathrm{B}}T)T^2\mathrm{e}^{-q\phi\beta}, \tag{2}$$

where E_{F} is the Fermi energy and v_F is the Fermi velocity. In our work, we set the value of v_F to 1×10^6 m/s for Dirac semimetal Cd_3As_2 according to an experiment result[19].

Based on thermionic emission processes, two kinds of devices, namely thermionic generators and thermionic coolers, have been proposed[3,20,21]. Thermionic generators show promising applications in harvesting thermal energy[22,23]. In addition, they have been used to convert solar energy to electricity[24]. The investigation of thermionic cooling can be dated

back to 1994, when G. D. Mahan described thermionic refrigeration[25]. The thermionic cooler is made of two parallel planes and a thermal barrier. Theoretically, the cooler can work as a room temperature refrigerator if the work function of its anode material is about 0.3 eV. A few years later, Mahan extended the work to multilayer thermionic refrigeration[26]. Some of our authors have obtained several results on thermionic cooling such as numerical calculation of thermionic cooling efficiency in a double-barrier semiconductor heterostructure[27]; electronic efficiency in nanostructured thermionic and thermoelectric devices[28], space charge effects in I-V characteristics of multilayer semiconductor thermionic devices[29] and high efficiency non-Richardson thermionics in three dimensional Dirac materials[17]. The results show space charge has considerable influence on thermionic devices, and the performance of thermionic performance can be improved by engineering the electron energy spectrum. We have found that 3D Dirac semimetals have the best thermal efficiency and coefficient of performance when compared to conventional semiconductors and graphene. Since the low emission current suffered in graphene due to the vanishing density of states is enhanced by an increased group velocity in 3D Dirac materials. Additionally, the thermal energy per degree of freedom carried by electrons in 3D Dirac materials is twice of that carried by an in electron in conventional materials. Recently, much work has been carried out to understand the thermionic emission in graphene systems and in Schottky heterostructures[30–39].

In the present work, we demonstrate that thermionic emission in 3D Dirac materials can be used to cool electronic devices effectively. Additionally, the energy (power) consumed by the process is low, and the cooling efficiency is high.

II. MODEL

A schematic diagram of electric devices without and with thermionic cooling is shown in Fig. 1(a) and (b), respectively. The red part of the centre plane is the heart of the electronic device that realizes all electronic functions, which is coated by a layer of insular materials indicated by yellow. The green outer layer of the centre plane is the cathode giving out thermionic emission, and its temperature is the internal temperature. The left and right planes are the boundaries of the device and provide mechanical protection. Between the centre plane and the boundary planes, there is a thermal barrier. This can be a vacuum gap or a barrier material. The centre plane will produce heat at a constant power P_{in} while the

device runs. For devices without thermionic cooling, the heat is transferred to the boundary planes by thermal radiation and thermal conduction. For device with thermionic cooling, the heat is also transferred to the boundary planes by thermionic cooling. In our model, the temperature of centre plane (the internal temperature, T) is assumed to be uniform, and the temperature of boundary planes (the environmental temperature, T_{E}) is assumed to be both uniform and constant. According to the Stefan-Boltzmann law, the thermal radiation heat is approximately given by $2A\epsilon\sigma(T^4 - T_{\mathrm{E}}^4)$, where $\sigma = 5.67 \times 10^{-8}$ Js^{-1}m^{-2}K^{-4} is the Stefan-Boltzmann constant, ϵ is the emissivity and $2A$ (here 2 for the left and right sides) is the surface area of the centre plane. The thermal conduction heat is given by $2AK(T - T_{\mathrm{E}})$, where K is the heat transfer coefficient. For the convenience of plotting, we set $K = aK_0$, where $K_0 = 2 \times 10^3$ W/cm^{2}K and a is a dimensionless parameter. In practical applications, the value of K can be varied by changing materials or the sample thickness. The thermionic cooling is realized by carefully choosing materials and applying an external voltage (V) between the centre plane and the boundary planes. We assume both centre and boundary planes are made up of the 3D Dirac material $\mathrm{Cd_3As_2}$. In our device, the thermionic cooling can be turned on and off by controlling the external voltage, while the thermal radiation and thermal conduction will always be present.

For thermionic based cooling devices, a small work function is always preferred since a smaller work function results in a higher thermionic emission current. However, the work function of typical materials is of order eV in bulk materials and a few hundred meV in low dimensional materials. In our calculations, we choose a relative low work function $q\phi = 250$ meV to demonstrate the thermionic effect. For a specific work function, there is an optimal external bias, which produces the highest thermionic cooling and efficiency. Here the optimal bias is $V = 55$ mV. Additionally, we assume the maximum running temperature of the electric devices is 40 °C.

III. RESULTS AND DISCUSSION

At the outset, we discuss the heat transfer in devices without thermionic cooling. The heat is transferred by two kinds of mechanism *i.e.* thermal radiation and thermal conduction. The whole heat transfer processes can be described by the following equation,

$$\Delta Q = mC_v\Delta T = AP_{\mathrm{in}}\mathrm{d}t - 2A\epsilon\sigma(T^4 - T_{\mathrm{E}}^4)\mathrm{d}t - 2AK(T - T_{\mathrm{E}})\mathrm{d}t, \tag{3}$$

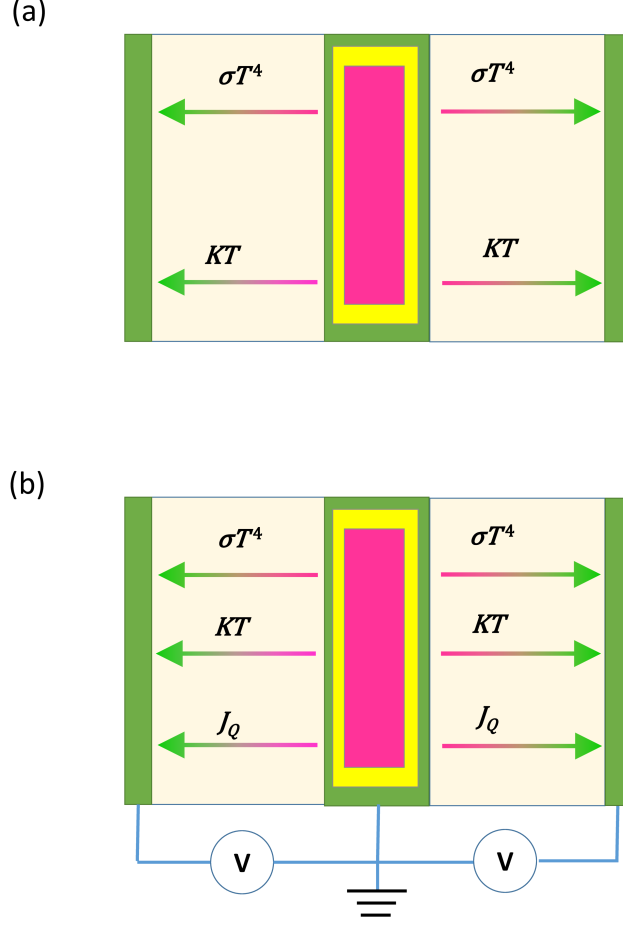

FIG. 1. (Color online) A schematic diagram of the electric devices (a) without thermionic cooling (b) with thermionic cooling. The red part of the centre plane is the heart of the device, which is coated by a layer of insular materials indicated by yellow. The green outer layer of the centre plane is the cathode giving out thermionic emission, and its temperature (T) is the internal temperature. The left and right planes are the boundaries of the device, which have constant temperature T_{E}, named as environmental temperature. The green part of the planes is made of Dirac semimetal. The centre green plane is grounded, and the green boundary planes are positively biased. The (a) and (b) have the same structure except for the external voltage.

where ΔQ is the heat change of the centre plane in a small period of time $\mathrm{d}t$, $m = \rho A d$ is the mass of the centre plane, $\rho = 3.03 \times 10^3$ kg/cm^3 is the volumetric mass density of $\mathrm{Cd_3As_2}$, $d = 1$ mm is the thickness of the centre plane, ΔT is the change of the internal temperature, K is the heat transfer coefficient, and C_v is the specific heat capacity of $\mathrm{Cd_3As_2}$. Since this

value is not available, we assume it can be approximately calculated by,

$$C_v = \frac{3m_{Cd}C_v^{Cd} + 2m_{As}C_v^{As}}{3m_{Cd} + 2m_{As}}, \tag{4}$$

where $C_v^{Cd} = 230$ J/kg K and $C_v^{As} = 330$ J/kg K are the specific heat capacity at room temperature of cadmium (Cd) and arsenic (As), respectively, and m_{Cd} and m_{As} are the standard atomic weights of Cd and As. The calculated C_v is 260 J/kg K, and we assume it is constant in our calculation. After some algebra, Eq. 3 can be rewritten as

$$\Delta T = \frac{2}{\rho d C_v}[\frac{P_{\mathrm{in}}}{2} - \epsilon\sigma(T^4 - T_{\mathrm{E}}^4) - K(T - T_{\mathrm{E}})]\mathrm{d}t, \tag{5}$$

where $P_{in} = 1$ W/cm^2 and $\epsilon = 0.5$. There are only two unknown parameters *i.e.* ΔT and $\mathrm{d}t$. Therefore, the time dependence of the internal temperature can be calculated.

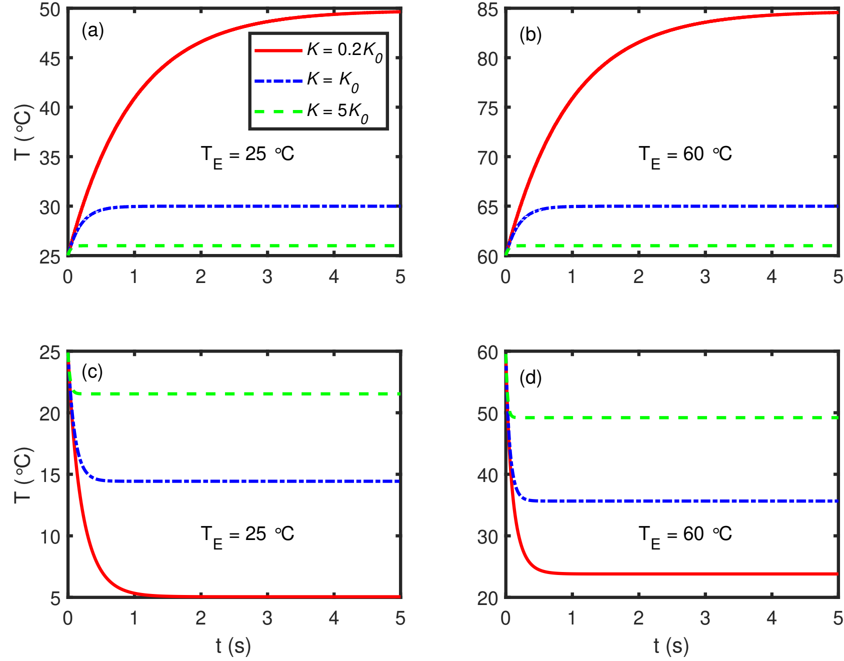

FIG. 2. (Color online) Time dependence of the internal temperature at three different values of K where (a), (b) for devices without thermionic cooling and (c), (d) for devices with thermionic cooling. $T_E = 25\,°\mathrm{C}$ for (a), (c) and $T_E = 60\,°\mathrm{C}$ for (b), (d). For all situations, the internal temperature reaches a saturation value and keeps constant after a few seconds.

The numerical results are shown in Fig. 2 (a) and (b) for $T_E = 25$°C and 60°C. In the present work, 40 °C is assumed to be the highest internal running temperature of the devices. For $K = 0.2K_0$ and $T_E = 25\,°\mathrm{C}$, the internal temperature reaches 40 °C in just one

second and then reaches a maximum temperature of 50 °C. When $T_E = 25$ °C, the maximum internal temperatures for $K = K_0$ and $K = 5K_0$ are about 30 °C and 26 °C, respectively, which indicates the devices running well at an environmental temperature $T_{\mathrm{E}} = 25$ °C. When $T_E = 60$ °C, the internal temperatures for three K are always greater than 40 °C, to be more precise, greater even than 60 °C. From the results, three conclusions can be drawn. Firstly, a large K is highly desirable in devices without thermionic cooling since it means better thermal conduction that can quickly transport heat into surroundings. Secondly, the internal temperature may reach the maximum temperature in just a few seconds. Lastly, no matter how large K is, the internal temperature is higher than or equal to the environmental temperature. Before the device is turned on, the internal temperature equals the environmental temperature. When the device is turned on, the internal temperature will gradually become higher than the environmental temperature. This feature considerably hinders the applications of the devices. For example, if the environmental temperature is higher than 40 °C, then the internal temperature will always be higher than the highest running temperature.

Now, we discuss the heat transfer in the devices with thermionic cooling. Unlike thermal radiation and thermal conduction, thermionic cooling can transport net heat from a cold object to a hot object[17]. This means the internal temperature can be lower than the environmental temperature. When thermionic cooling is introduced, Eq. 5 can be rewritten as,

$$\Delta T = \frac{2}{\rho d C_v}[\frac{P_{\mathrm{in}}}{2} - \epsilon\sigma(T^4 - T_{\mathrm{E}}^4) - K(T - T_{\mathrm{E}}) - J_Q]\mathrm{d}t, \tag{6}$$

where J_Q is the heat flow contributed by thermionic cooling, given by[17]

$$J_Q = [(q\phi + 4k_{\mathrm{B}}T)J(T) - (q\phi + 4k_{\mathrm{B}}T_{\mathrm{E}})J(T_{\mathrm{E}})\mathrm{e}^{qV\beta}]/q. \tag{7}$$

The time dependence of the internal temperature at three values of K is shown in Fig. 2(c) for $T_{\mathrm{E}} = 25$ °C and (d) for $T_{\mathrm{E}} = 60$ °C. When $T_E = 25$ °C, the internal temperatures for three values of K are well below 40 °C. When $T_E = 60$ °C, the maximum internal temperature is about 24 °C and 36 °C for $K = 0.2K_0$ and $K = K_0$, respectively, indicating that the thermionic enhanced devices can run well at $T_{\mathrm{E}} = 60$ °C. For $K = 5K_0$, the maximum internal temperature is lower than the environmental temperature and higher than the highest running temperature. In devices without thermionic cooling, a large K results in a low internal temperature. However, in thermionic enhanced devices, a large K results in

a high internal temperature. The fundamental reason is that the internal temperature is lower than the environmental temperature in thermionic enhanced devices. In such devices, a large K accelerates the heat conduction from the surroundings to the interior of the devices, leading to a high internal temperature. Therefore, in thermionic enhanced devices, a small K is wanted instead of a large one. Additionally, the internal temperature reaches the maximum temperature in one second.

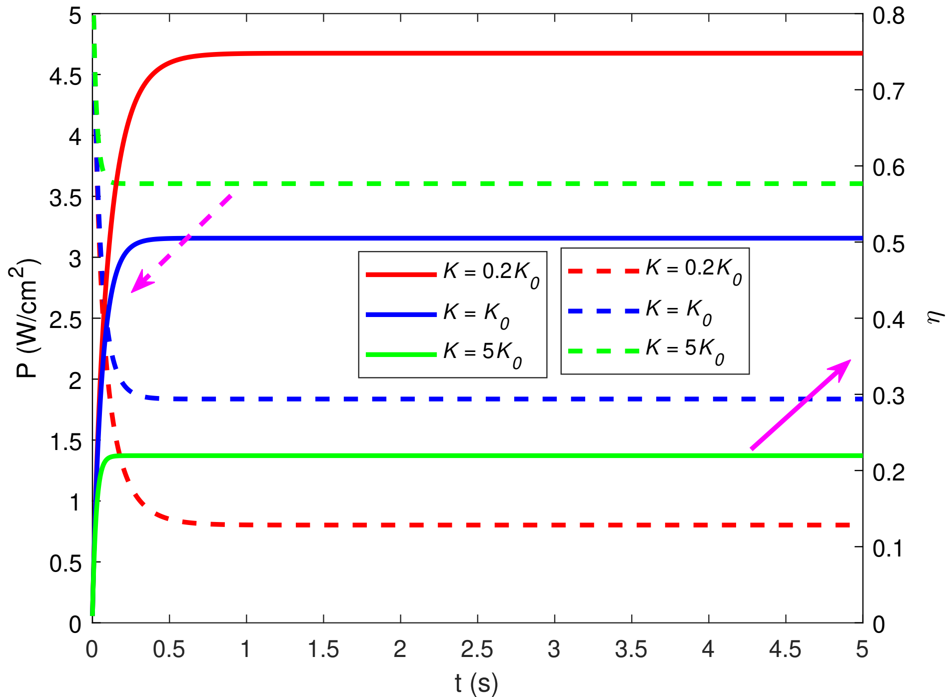

FIG. 3. (Color online) Time dependence of the consumed power in thermionic cooling process (dashed line with left y-axis as indicated by the magenta dashed arrow) and the cooling energy efficiency (solid line with right y-axis as indicated by the magenta solid arrow), where $T_{\mathrm{E}} = 60\,^{\circ}\mathrm{C}$.

In thermionic enhanced devices, an external voltage is needed to drive the thermionic cooling, which consumes energy. The consumed power density P can be calculated by,

$$P = J_{net}V, \tag{8}$$

where the $J_{net} = 2[J(T) - J(T_{\mathrm{E}})\mathrm{e}^{qV\beta}]$ is the net current density. The time dependence of P is shown in Fig. 3 with the dashed curves, where $T_E = 60\,^{\circ}\mathrm{C}$. The curves share a similar trend with those in Fig. 2(c) and (d). The reason is that P depends only on T when V and

$T_{\rm E}$ are fixed. Therefore, P and T share a similar time dependence. Combining Fig. 2 and Fig. 3, we find the device with the smallest K has the best performance in the thermionic cooling process, having the lowest internal temperature and the smallest consumed power. The underlying reason is found in Eq. 8, where a smaller T leads to a smaller P.

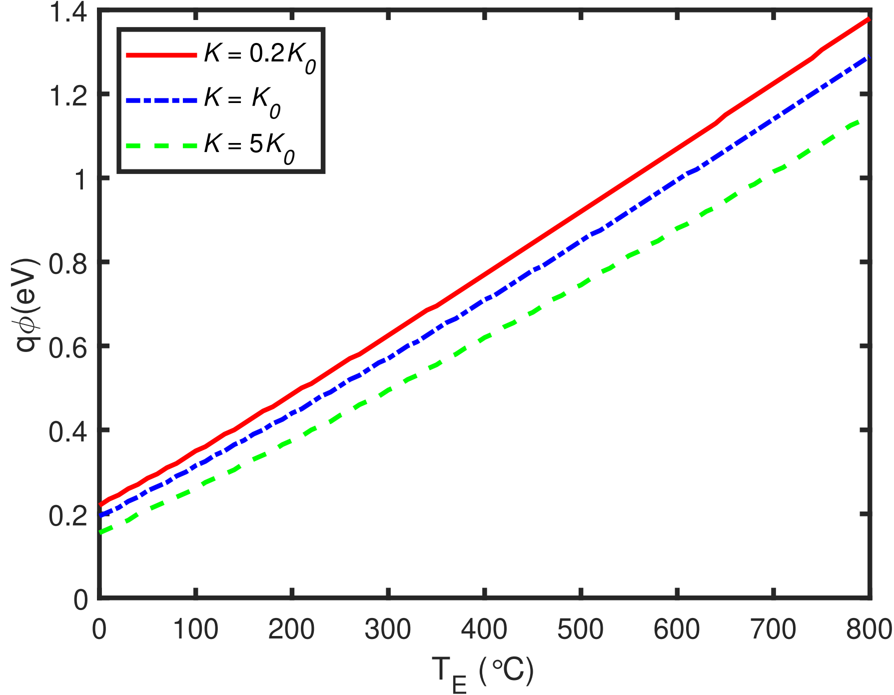

FIG. 4. (Color online) The minimum work function ($q\phi$) as a function of environmental temperature (T_E) at three values of K, where $V = 60$ mV and $T - T_E = 20$ K.

In order to characterize the cooling energy efficiency of the thermionic enhanced devices, a relative efficiency is defined as,

$$\eta = \frac{J_Q}{P} \times \frac{T_{\rm E} - T}{T}, \tag{9}$$

where $T/(T_{\rm E} - T)$ is the Carnot efficiency. According to the equation, the time dependence of η is plotted in Fig. 3 with the solid curves. The results show that η decreases with K, which indicates again that the thermionic enhanced device with the smallest K has the best performance in thermionic cooling. The energy efficiency is rather high, up to 75% of the Carnot efficiency. However, we should point out that the device with the smallest K has a rather low T_{c1}, and this limits the applications of the device.

Thermionic emission current is sensitive to the work function and the temperature. In order to generate enough thermionic cooling, there is a minimum work function for a specific work temperature. The minimum work function *vs* T_E is plotted in Fig. 4, where $V = 70$ mV and $T_E - T = 20$ K. Here a relative larger external voltage is used to obtain the maximum thermionic emission current for all work functions. The difference between T_E and T keeps constant for all work functions. The results show the minimum work function considerably depends on T_E. In Eq. 2, the thermionic emission current is mainly determined by the exponent part $\mathrm{e}^{-q\phi\beta}$, which results in a linear temperature dependence of the work function. Additionally, there is a nonlinear part $q\phi + E_F + 2k_BT$. This is why a quasi-linear T_E dependence of $q\phi$ is observed.

IV. CONCLUSION

We have shown that the thermionic effect can be employed to enhance heat transfer in electronic devices. With thermionic cooling, the internal temperature of the devices may be considerably lower than the surrounding environmental temperature. In this sense, the operating temperature range of the devices may be significantly extended. The energy consumed by thermionic cooling and its energy efficiency are consonant with an excellent heat transfer performance. These findings promise to be useful in developing future electronic devices.

ACKNOWLEDGMENTS

The work was supported by the Australian Research Council (Grant DP160101474).

REFERENCES

[1] R. Rhyner and M. Luisier, Nano Letters **16**, 1022 (2016).

[2] S. V. Garimella, Y. K. Joshi, A. Bar-Cohen, R. Mahajan, K. Toh, V. Carey, M. Baelmans, J. Lohan, B. Sammakia, and F. Andros, IEEE Transactions on Components and Packaging Technologies **25**, 569 (2002).

[3] M. F. O'Dwyer, R. A. Lewis, and C. Zhang, Journal of Physics D: Applied Physics **40**, 1167 (2007).

[4] C. Huang, Y. Pan, Y. Wang, G. Su, and J. Chen, Energy Conversion and Management **121**, 186 (2016).

[5] T. Shinozaki, S. Hagiwara, N. Morioka, Y. Kimura, and K. Watanabe, Applied Physics Express **11**, 064301 (2018).

[6] F. A. Koeck, R. J. Nemanich, A. Lazea, and K. Haenen, Diamond and Related Materials **18**, 789 (2009).

[7] J. Domenech-Garret, S. Tierno, and L. Conde, The European Physical Journal B **86**, 382 (2013).

[8] J. Ryan Smith, Journal of Applied Physics **114**, 164514 (2013).

[9] S. Borisenko, Q. Gibson, D. Evtushinsky, V. Zabolotnyy, B. Büchner, and R. J. Cava, Physical Review Letters **113**, 027603 (2014).

[10] S. Huang, M. Sanderson, J. Tian, Q. Chen, F. Wang, and C. Zhang, Journal of Physics D: Applied Physics **51**, 015101 (2017).

[11] S. S. Kubakaddi and T. Biswas, Journal of Physics: Condensed Matter **30**, 265303 (2018).

[12] L. He, X. Hong, J. Dong, J. Pan, Z. Zhang, J. Zhang, and S. Li, Physical Review Letters **113**, 246402 (2014).

[13] Q. Wang, C.-Z. Li, S. Ge, J.-G. Li, W. Lu, J. Lai, X. Liu, J. Ma, D.-P. Yu, Z.-M. Liao, and D. Sun, Nano Letters **17**, 834 (2017).

[14] I. Crassee, R. Sankar, W.-L. Lee, A. Akrap, and M. Orlita, Physical Review Materials **2**, 120302 (2018).

[15] C. Zhu, F. Wang, Y. Meng, X. Yuan, F. Xiu, H. Luo, Y. Wang, J. Li, X. Lv, L. He, Y. Xu, L. Junfeng, C. Zhang, Y. Shi, R. Zhang, and S. Zhu, Nature Communications **8**, 14111 (2017).

[16] C. Zhang, T. Zhou, S. Liang, J. Cao, X. Yuan, Y. Liu, Y. Shen, Q. Wang, J. Zhao, Z. Yang, and F. Xiu, Chinese Physics B **25**, 017202 (2015).

[17] S. Huang, M. Sanderson, Y. Zhang, and C. Zhang, Applied Physics Letters **111**, 183902 (2017).

[18] X. Zhang, W. Peng, G. Su, S. Su, and J. Chen, Journal of Physics D: Applied Physics **51**, 405501 (2018).

[19] Y. Liu, C. Zhang, X. Yuan, T. Lei, C. Wang, D. Di Sante, A. Narayan, L. He, S. Picozzi, S. Sanvito, *et al.*, NPG Asia Materials **7**, e221 (2015).

[20]R. Y. Belbachir, Z. An, and T. Ono, Journal of Micromechanics and Microengineering **24**, 085009 (2014).

[21]F. Morini, E. Dubois, J.-F. Robillard, S. Monfray, and T. Skotnicki, Physica Status Solidi (a) **211**, 1334 (2014).

[22]K. A. A. Khalid, T. J. Leong, and K. Mohamed, IEEE Transactions on Electron Devices **63**, 2231 (2016).

[23]X. Zhang, Y. Pan, and J. Chen, IEEE Transactions on Electron Devices **64**, 4594 (2017).

[24]D. M. Trucchi, A. Bellucci, M. Girolami, P. Calvani, E. Cappelli, S. Orlando, R. Polini, L. Silvestroni, D. Sciti, and A. Kribus, Advanced Energy Materials **8**, 1802310 (2018).

[25]G. Mahan, Journal of Applied Physics **76**, 4362 (1994).

[26]G. Mahan and L. Woods, Physical Review Letters **80**, 4016 (1998).

[27]B. Lough, S. Lee, R. Lewis, and C. Zhang, Physica E: Low-dimensional Systems and Nanostructures **11**, 287 (2001).

[28]M. F. O'Dwyer, R. A. Lewis, C. Zhang, and T. E. Humphrey, Physical Review B **72**, 205330 (2005).

[29]B. Lough, S. Lee, Z. Dou, R. Lewis, and C. Zhang, Physica E: Low-dimensional Systems and Nanostructures **17**, 651 (2003).

[30]M. Bescond, D. Logoteta, F. Michelini, N. Cavassilas, T. Yan, A. Yangui, M. Lannoo, and K. Hirakawa, Journal of Physics: Condensed Matter **30**, 064005 (2018).

[31]F. Jin and D. Carter, Journal of Vacuum Science & Technology B, Nanotechnology and Microelectronics: Materials, Processing, Measurement, and Phenomena **36**, 051804 (2018).

[32]F. Jin and S. Little, Applied Physics Letters **106**, 113102 (2015).

[33]S.-J. Liang, B. Liu, W. Hu, K. Zhou, and L. Ang, Scientific Reports **7**, 46211 (2017).

[34]Y. Ang, S.-J. Liang, and L. Ang, MRS Bull **42**, 505 (2017).

[35]S.-J. Liang and L. Ang, Physical Review Applied **3**, 014002 (2015).

[36]M. Trushin, Applied Physics Letters **112**, 171109 (2018).

[37]M. Trushin, Physical Review B **97**, 195447 (2018).

[38]Y. S. Ang, H. Y. Yang, and L. Ang, Physical Review Letters **121**, 056802 (2018).

[39]Y. S. Ang, Y. Chen, C. Tan, and L. Ang, Physical Review Applied **12**, 014057 (2019).